REVISTA MATÉRIA V.29 N.1
ISSN 1517-7076 articles e20230311, 2024

# Effect of heat treatment on the microstructure and surface damage evolution of selective-laser-melted IN718 alloy

Lei Li[1], Xiaodong Li[1], Qiao Liu[1], Dexin Mao[1]

[1]Inner Mongolia University of Technology, College of Sciences. Aimin Street, 49, 010051, Xincheng District, Hohhot, PR China.

e-mail: leillt@163.com, 1774837317@qq.com, 1097555026@qq.com, 2582887978@qq.com

## ABSTRACT

The microstructure and damage evolution behavior of IN718 alloy prepared by selective laser melting (SLM, referred to as SLM IN718 alloy) under different heat treatment processes were studied using optical microscopy, scanning electron microscopy, electron backscatter diffraction, microhardness tests, and other material tests, combined with digital image correlation. The heat treatment of the SLM IN718 alloy achieved different degrees of recrystallization and transformed the microstructure from dendritic crystals to bulk crystals with the precipitation of a large number of γ′ and γ″ phases. As the heat-treatment temperature was increased, the δ phase of the SLM IN718 alloy was precipitated and then dissolved, the microhardness and strength of SLM IN718 alloy increased and then decreased, the elongation decreased and then increased, and toughness fracture was the main fracture mode. Therefore, heat treatment can be used to alter the relative proportions of recrystallized and substructured grains in the SLM IN718 alloy, thereby modulating its overall mechanical properties. After heat treatment, the damage factor entered the rapid damage stage earlier, and the critical damage factor increased as the critical plastic strain was increased. Further, the damage evolution equations of the SLM IN718 alloy under different heat treatment processes were established.

**Keywords:** Selective-laser-melted IN718 alloy; heat treatment; damage evolution; digital image correlation; microstructure.

## 1. INTRODUCTION

Selective laser melting (SLM) is an additive manufacturing technology with the advantages of high material utilization, short production cycle, and direct construction of metal components of arbitrary complex shapes; thus, it is successfully applied for the manufacture of a wide range of metal parts [1–5]. IN718 alloy is a nickel–chromium–iron precipitation-hardened alloy with niobium and molybdenum and has been extensively used in aerospace and nuclear industries because of its exceptional mechanical behavior at high temperatures and corrosion resistance [6, 7]. The SLM of IN718 alloys overcomes the limitations of traditional machining and manufacturing methods, including the long manufacturing cycle time and difficulty in machining complex parts, thereby providing a new approach for the design and manufacture of IN718 alloy components [8, 9]. However, the molding process of the SLM technology with repeated heating and rapid solidification usually results in defects, such as high residual stresses, suppressed precipitation phases, and microcracking, decreasing the fatigue performance, yield strength, and tensile strength of the resulting components [10–12].

Heat treatment is an important method for optimizing the microstructure and mechanical properties of metallic materials. HE [13] performed solution and double-aging heat treatment for the rapid laser prototyping of the IN718 alloy and found that its yield and tensile strengths significantly improved after heat treatment, whereas the ductility and elongation decreased. CHLEBUS *et al.* [14] performed a double-aging heat treatment on an SLM-fabricated IN718 alloy (hereafter, simply referred to as SLM IN718 alloy), noting that heat treatment did not completely eliminate the texture. Moreover, the yield strength, tensile strength, and hardness of the aged SLM IN718 alloy were slightly higher than those of the wrought alloy, and the elongation values slightly decreased but remained satisfactory. ZHAO *et al.* [15] performed solid-solution and aging heat treatment on an SLM IN718 alloy. The precipitation of the γ″ strengthening phase can be further optimized and the corresponding mechanical properties of the SLM IN718 alloy improved significantly by adjusting the aging treatment conditions. In particular, the elongation of the SLM IN718 alloy at room temperature significantly increased

Corresponding Author: Xiaodong Li Received on 02/11/2023 Accepted on 08/01/2024

DOI: https://doi.org/10.1590/1517-7076-RMAT-2023-0311

to 29% with a slight decrease in strength. ZHANG *et al.* [16] conducted different aging heat treatments on an SLM IN718 alloy. The mechanical properties of the SLM IN718 alloy after aging treatment improved compared to those of the as-deposited alloy. In particular, the strength and hardness of the SLM IN718 alloy tended to increase and then decrease with the aging time.

Digital image correlation (DIC) is a photomechanical method used to obtain the strain field on the material surface by comparing the change in the speckle field on the surface before and after material deformation and applying a relevant calculation method [17, 18]. This method is widely used in various scientific fields because it allows the full-field strain measurements of materials in noncontact situations. POPOVICH *et al.* [19] studied the damage process of an IN718 alloy using DIC, determining that hot isostatic pressing did not affect its microstructure. Moreover, the strain evolutions of the samples before and after different heat treatments were similar. OKEIL *et al.* [20] applied DIC to the axial tensile tests of deformed reinforcement bars embedded in concrete and cement paste samples, revealing the differences in the surface crack expansion of the reinforcement bars. WEI *et al.* [21] exhibited the surface damage evolution of a Cu alloy using DIC. SI *et al.* [22] combined DIC and acoustic emission to monitor the fatigue damage process in TC4 alloys. The combination of both methods effectively obtained the fatigue damage condition of the structural components and monitored the fatigue crack activity online.

Although the effect of heat treatment on the microstructure and mechanical properties of SLM IN718 alloys has been extensively studied, its effect on the damage evolution of SLM IN718 alloys has rarely been analyzed using DIC. Therefore, this study conducted tensile tests on SLM IN718 alloy after different heat treatment processes and used DIC. The damage evolution of the SLM IN718 alloy was determined, and a damage evolution equation was established. The relationship between the damage evolution and macroscopic deformation of the SLM IN718 alloy was revealed. This study provides a reference for optimizing the heat treatment system of SLM IN718 alloys.

## 2. MATERIALS AND METHODS

### 2.1. Materials and sample preparation

EP-M250 equipment was used to prepare the SLM IN718 alloy with the chemical composition listed in Table 1. Under Ar atmosphere, the substrate was preheated to 80 °C to release the residual stresses generated by the fabrication between the SLM IN718 alloy and substrate plate using strip scanning. The laser power was 285 W, the scanning speed was 960 mm/s, and the interlayer angle was 67°. The material-forming details are shown in Figure 1. The prepared SLM IN718 alloy strip samples with a thickness of 1.5 mm were cut into dog-bone-shaped tensile samples by wire electrical discharge machining (AG400L) with the dimensions shown in Figure 2.

### 2.2. Heat treatment

For the heat treatment, the tensile samples of the SLM IN718 alloy were placed in a pipe furnace (SG-GL1200) at room temperature and heated at a rate of 5 °C/min until reaching the required temperatures. The samples were subjected to three different heat treatments, namely, double-aging heat treatment (denoted as DA), solution and double-aging heat treatment (denoted as SDA), and homogenization and double-aging heat treatment (denoted as HDA). The specific heat treatment conditions are shown in Table 2.

### 2.3. Test methods

The Vickers microhardness of the samples was obtained using a digital microhardness tester (Figure 3) with a test force of 9.8 N and holding time of 10 s. Ten microhardness data points were randomly taken from each sample and statistically analyzed to obtain the average value.

The samples were corroded using a metallographic etching solution ($HCl:C_2H_5OH:CuCl_2$ ratio of 100 mL:100 mL:5 g). The microstructures were observed by optical microscopy (OM; LEICA DM6 M) and scanning electron microscopy (SEM; QUANTA FEG650). The samples were subjected to electrolytic polishing

**Table 1:** Chemical composition of the SLM IN 718 alloy (wt%).

| C | Si | Mn | S | P | Cr | Ni |
|---|---|---|---|---|---|---|
| 0.05 | 0.043 | 0.03 | 0.002 | 0.034 | 19.01 | 52.30 |
| **Al** | **Nb** | **Ti** | **Cu** | **B** | **Mo** | **Fe** |
| 0.57 | 5.07 | 1.00 | 0.02 | 0.003 | 3.06 | Bal |

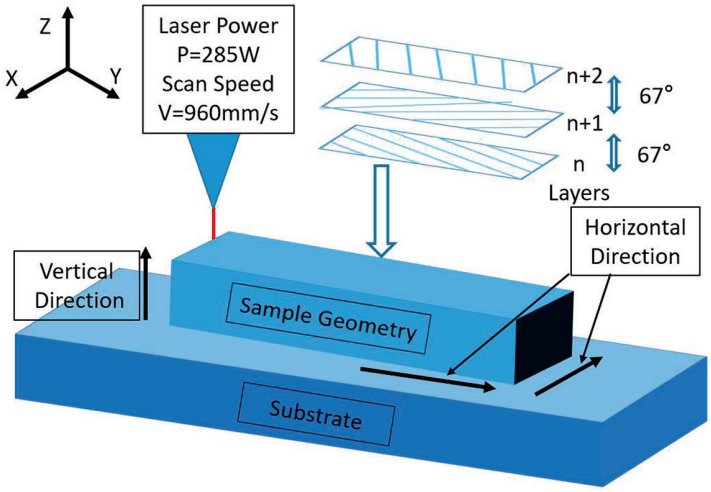


**Figure 1:** Schematic of the SLM **IN718** alloy deposition.

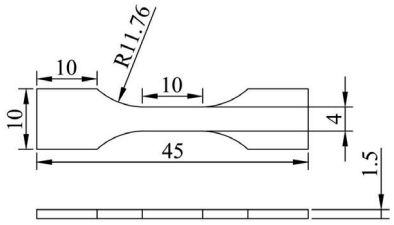


**Figure 2:** Dimension of the tensile samples (mm).

**Table 2:** Heat treatment conditions of the samples.

| SAMPLE | HEAT TREATMENT PROCESS |
|---|---|
| DA | 720 °C for 8 h/FC at 620 °C for 8 h/AC |
| SDA | 980 °C for 1.5 h/ AC at 720 °C for 8 h/FC at 620 °C for 8 h/AC |
| HDA | 1080 °C for 1.5 h/ AC at 720 °C for 8 h/FC at 620 °C for 8 h/AC |

Note: FC: furnace cooling, AC: air cooling.

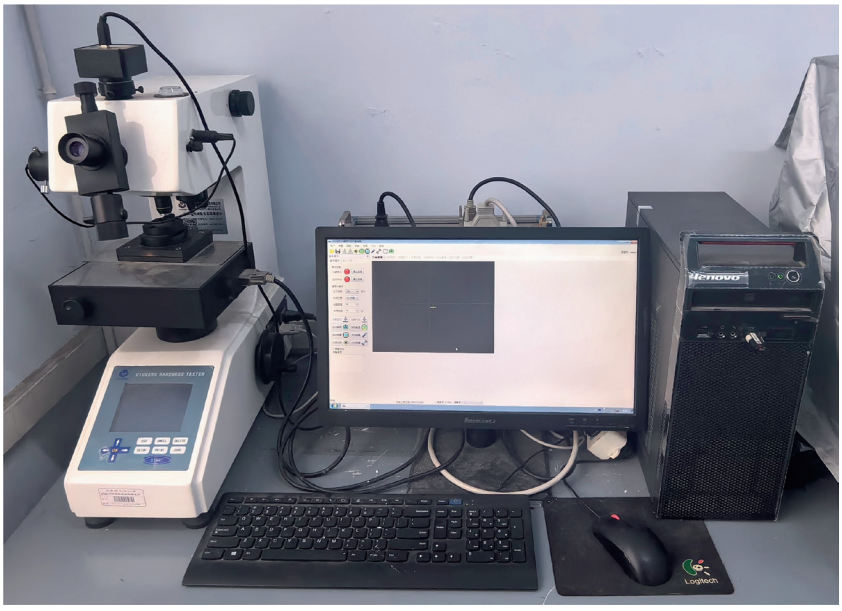

**Figure 3:** Microhardness test.


**Figure 4:** Tensile and DIC test.

using 10% $HClO_4$ + 90% $C_2H_5OH$ as the electrolytic polishing solution with the polishing voltage of 25 V, polishing temperature of −20 to −30 °C, and electrolytic polishing time of 45–60 s. Electron backscatter diffraction (EBSD) was performed on electrolytically polished samples to observe their internal microstructures.

Speckle spray treatment was applied by spraying a series of irregular DIC scatter test speckles onto the sample surface using black matte paint. The tensile tests of the samples were conducted at room temperature by a Landmark mechanical property tester at a tensile rate of 1 mm/min. During the tensile test, a charge-coupled device camera was set to take photographs every 1 s for the DIC (Figure 4).

## 3. RESULTS AND DISCUSSION

### 3.1. Microstructure

Figure 5 shows the microstructure of the SLM IN718 alloy. The as-deposited sample has a fine and compact organization with obvious melting marks and a large number of fine dendrites and columnar crystals distributed alternately. The dendritic crystals inside the DA sample transformed into block crystals, and the melt marks gradually faded. Meanwhile, the melt marks on the SDA sample completely disappeared, the segregation structure was dissolved, the grains coarsened, and the microstructure was relatively uniform. The HDA sample achieved complete recrystallization. In particular, its columnar crystals and dendrites disappeared and were replaced by large equiaxed crystals with noticeable grain coarsening and straightened grain boundaries.

Figure 6 shows the SEM micrographs of the SLM IN718 alloy. At the intersection of the scanned strips, the as-deposited sample exhibits alternating distributions of coarse dendrites in a honeycomb shape and fine dendrites in long strips with different orientations. Numerous white linear Laves phases precipitated, forming a

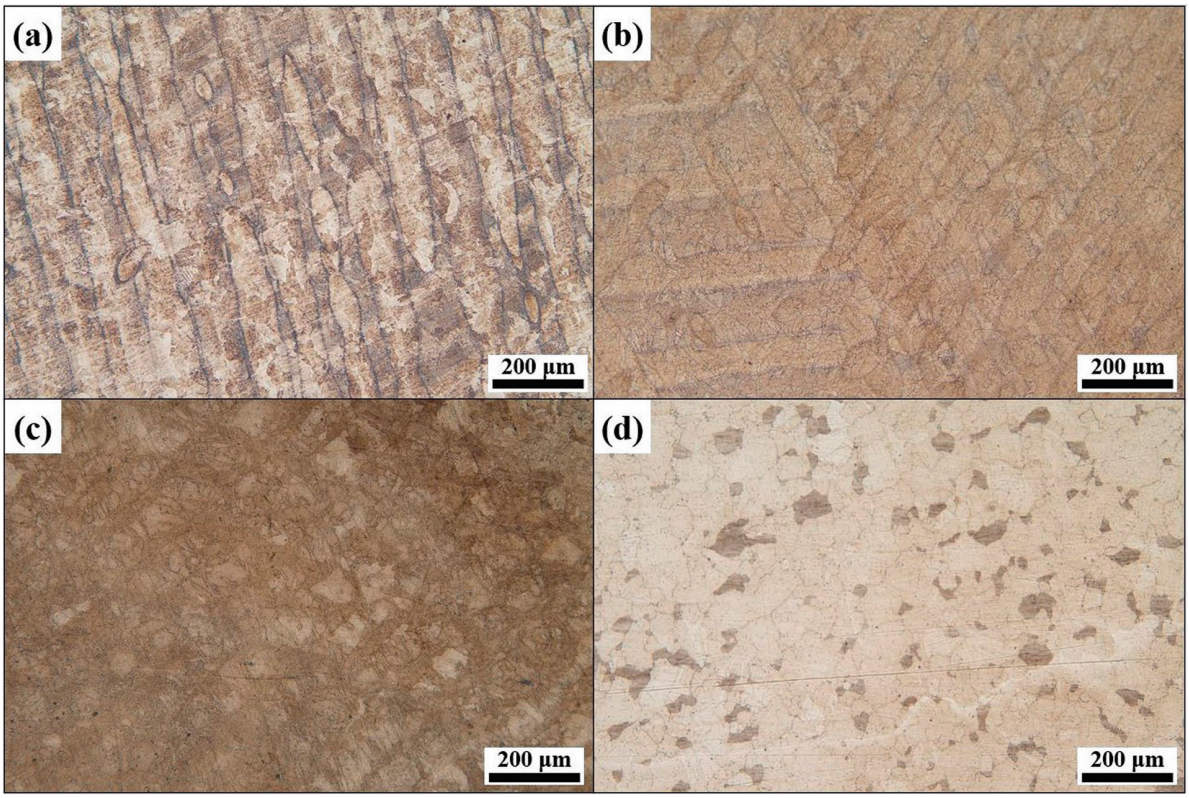


**Figure 5:** Microstructure of the SLM IN718 alloy: (a) as-deposited, (b) DA, (c) SDA, and (d) HDA.

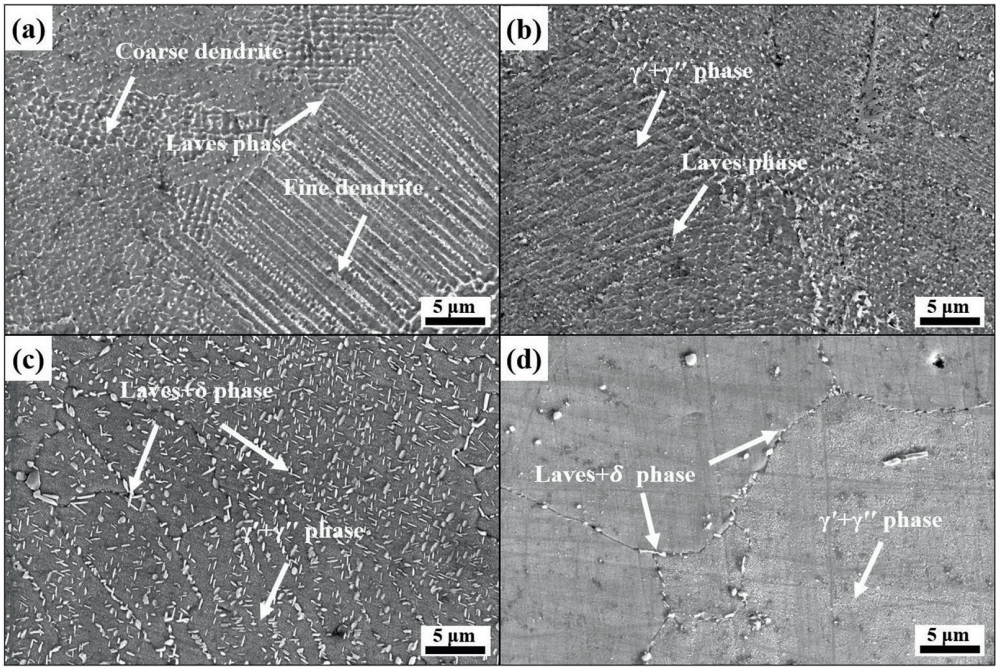


**Figure 6:** SEM micrographs of the SLM IN718 alloy: (a) as-deposited, (b) DA, (c) SDA, and (d) HDA.

clear boundary between the dendritic regions. The DA sample exhibits a more inhomogeneous overall structure with a higher number of precipitated phases. Among them, the Laves phase is distributed in long strips or rings, whereas the γ′ and γ″ phases are precipitated in large quantities. A large number of Laves phases is dissolved in the SDA sample, whereas short rods or needles of δ phases are precipitated. A large amount of δ phase is

dissolved in the HDA sample, and the hindering effect for the grain boundary migration decreases, thereby greatly coarsening the grains.

Figure 7 shows the orientation morphology obtained by EBSD (inverse pole figure (IPF)) of the SLM IN718 alloy after different heat treatments. In the remelting area, the grain domains of the DA sample grain domains owing to the diffusion of heat flow to the surrounding solidified metal, thereby disrupting its growth in the <001> direction. The growth direction became complex and variable with both the parallel growth of columnar crystals and varying sizes of equiaxial crystals. The SDA sample has a checkerboard-like structure with a more uniform grain distribution compared to the DA sample; however, their grain orientation patterns are similar. The grains in the HDA sample coarsen with flat boundaries and several annealing twins. The large number of highly angular-oriented twin boundaries in the material indicates the increase in the orientation difference between the grains in the material.

Figure 8 shows the distribution of the recrystallized microstructure of the SLM IN718 alloy after different heat treatments. The DA and SDA samples have similar internal microstructural distributions, which are

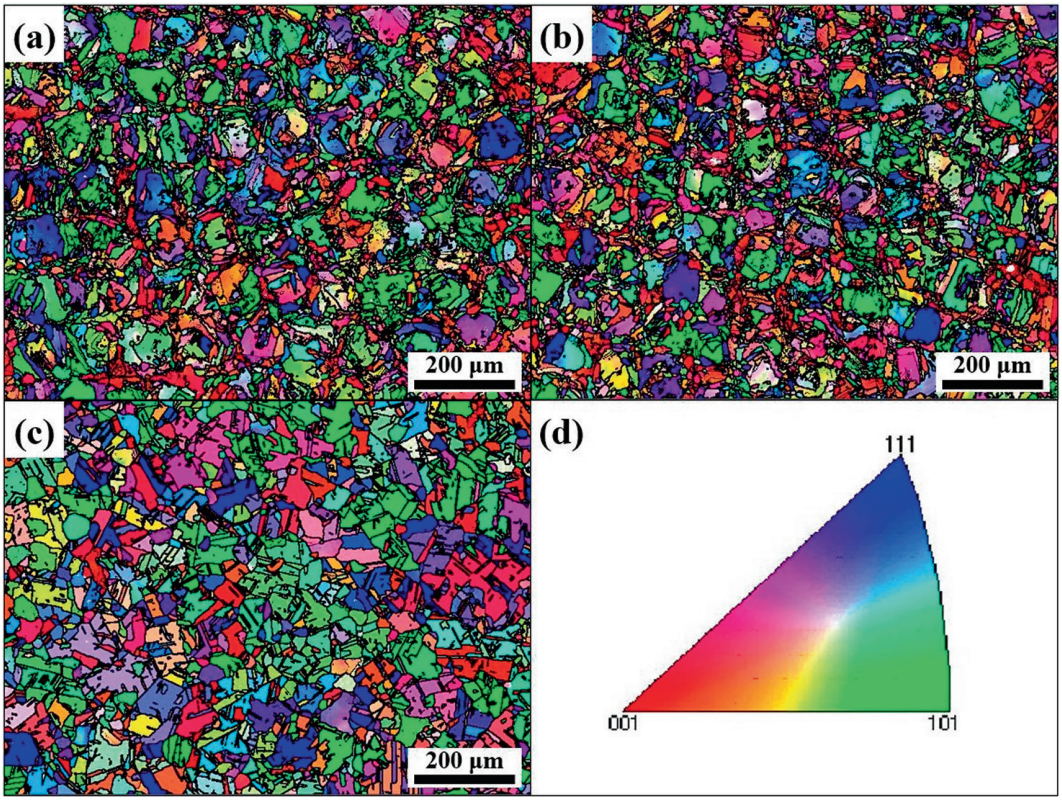


**Figure 7:** IPF images of the grain structures obtained by different heat treatments: (a) DA, (b) SDA, and (c) HDA. (d) IPF legend.

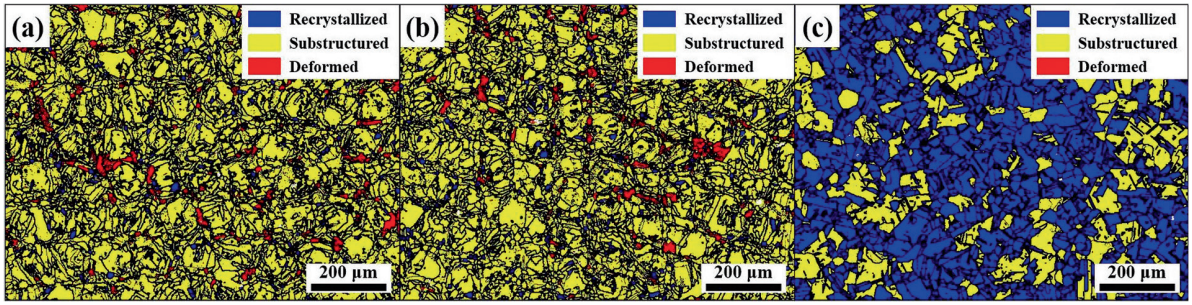


**Figure 8:** Distribution of the recrystallized microstructure of the SLM IN718 alloy after different heat treatments: (a) DA, (b) SDA, and (c) HDA.

**Table 3:** Volume fractions of recrystallized, substructured, and deformed grains in the SLM IN718 alloy after different heat treatments (%).

| SAMPLE | RECRYSTALLIZED | SUBSTRUCTURED | DEFORMED |
|---|---|---|---|
| DA | 6.2 | 86.1 | 7.7 |
| SDA | 7.9 | 85.8 | 6.3 |
| HDA | 72.3 | 27.6 | 0.1 |

predominantly substructured grain with few recrystallized and deformed grains. The HDA sample has a large number of recrystallized grains and a certain number of substructured grains with almost no deformed grains. The volume fractions of the recrystallized, substructured, and deformed grains in the microstructure of the SLM IN718 alloy after different heat treatments are shown in Table 3. The heat treatment of DA to HDA increased the recrystallized volume fraction from 6.2% to 72.3% and decreased the substructured volume fraction from 86.1% to 27.6% and the deformed grain volume fraction from 7.7% to 0.1%. Therefore, heat treatment facilitates the internal organization of the material from substructured grains the recrystallized grains. As the heat-treatment temperature was increased, more the recrystallized grains are transformed.

Figure 9 shows a kernel average misorientation (KAM) map of the SLM IN718 alloy after different heat treatments. The KAM map consists of 24 neighboring points, and the orientation difference between the core and neighboring points indicates the local orientation difference, which indicates the residual stresses within the material, that is, as the orientation difference increases, the residual stresses are more concentrated [23]. The green area in Figure 9 shows the area of the residual stress concentration. The internal residual stresses of the SLM IN718 alloy improved to different degrees with heat treatment. The residual stress distribution states of the DA, SDA, and HDA samples are essentially identical, and the residual stresses are concentrated in and around the deformed grains. The DA and SDA samples exhibit a more pronounced residual stress. The deformed grains with high localized orientation difference in the HDA samples almost disappeared with minimal residual stress. Thus, the residual stress inside the SLM IN718 alloy can be eliminated through heat treatment.

### 3.2. Mechanical properties

Figure 10 shows the microhardness of the SLM IN718 alloy. The microhardness of the SLM IN718 alloy after three heat treatments is significantly improved from that of the as-deposited sample. After heat treatment, a large number of γ′ and γ″ phases are precipitated, acting as reinforcement, thereby providing good structural stability and significantly increasing the microhardness of the sample [24, 25]. The SDA sample had the highest microhardness of 483.981 HV. Meanwhile, the microhardness of the HDA sample is lower that of the SDA sample owing to the significant dissolution of the δ phase, enlarged grains, and complete release of residual stresses.

The stress–strain curve of the SLM IN718 alloy is shown in Figure 11, and the mechanical properties are shown in Table 4. The as-deposited sample has the highest plasticity with an elongation of 21.6% but the lowest strength with a tensile strength of 911 MPa. After heat treatment, the strength of the SLM IN718 alloy greatly increased and the plasticity decreased owing to the considerable precipitation of the γ′ and γ″ phases, which have good microstructural stability [24]. The SDA sample has the highest tensile strength of 1497 MPa but the lowest plasticity with the elongation of approximately 8.3% because of the large quantities of dissolved Laves phases, further diffusion of solute elements, and homogeneous precipitation of a large number of δ phases inside the crystals and at the grain boundaries. The δ phase promoted the dislocation pinning in the matrix, hindering dislocation movement and greatly decreasing the elongation while increasing the strength of the SLM IN718 alloy [25–28]. The HDA sample has lower strength and higher plasticity than that of the SDA sample. The microstructure is dominated by recrystallized grains owing to the massive dissolution of the δ phase. A large number of annealing twins appeared, and the grains coarsened. Moreover, the precipitated phase is insufficient for strengthening the grain boundaries, thereby decreasing the strength and increasing the plasticity [29].

As shown in Table 4, the product of the strength and elongation after heat treatment is 18.1 GPa% when the volume fractions of recrystallized grains and substructured grains in the DA sample are 6.2% and 86.1%, respectively. The product of the strength and elongation for the DA sample is 12.4 GPa% for the volume fractions of 7.9% and 85.8% for the recrystallized and substructured grains, respectively. For the HDA sample, the volume fractions of recrystallized and substructured grains are 72.3% and 27.7%, respectively, and the product of strength and elongation reached 22.2 GPa%. As the elongation of the recrystallized grains improved, the toughness of the substructured grains increases owing to their high dislocation density. For the HDA sample, both microstructures have high volume fractions, resulting in the highest product of strength and elongation.

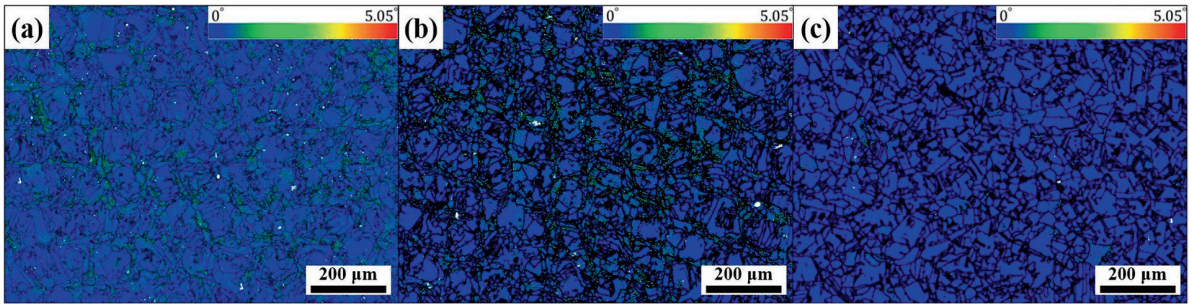


**Figure 9:** KAM of the SLM IN718 alloy after different heat treatments: (a) DA, (b) SDA, and (c) HDA.

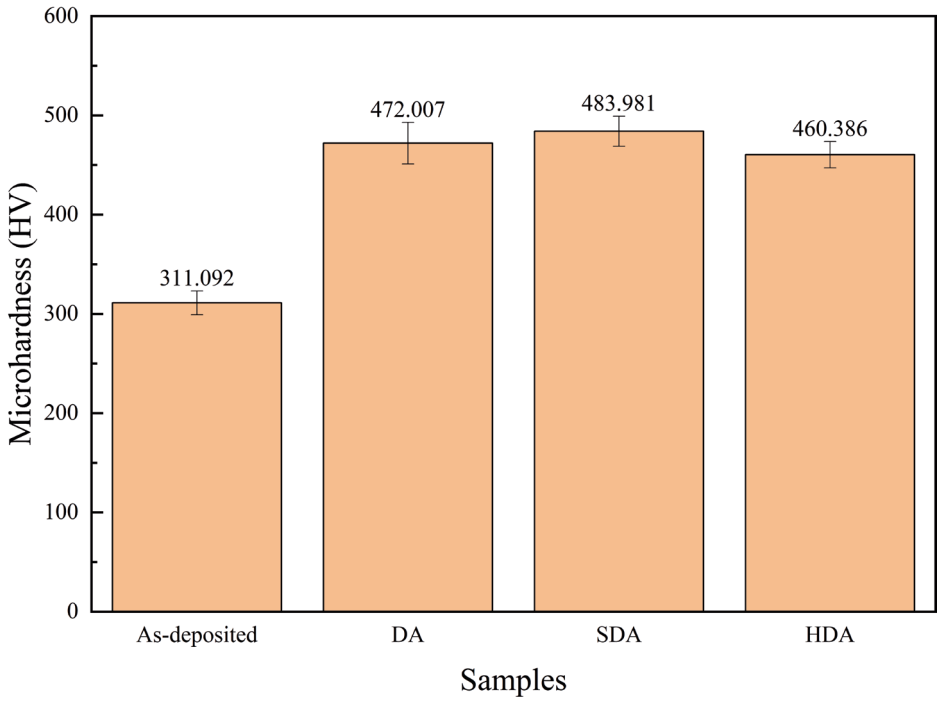


**Figure 10:** Microhardness of the SLM IN718 alloy.

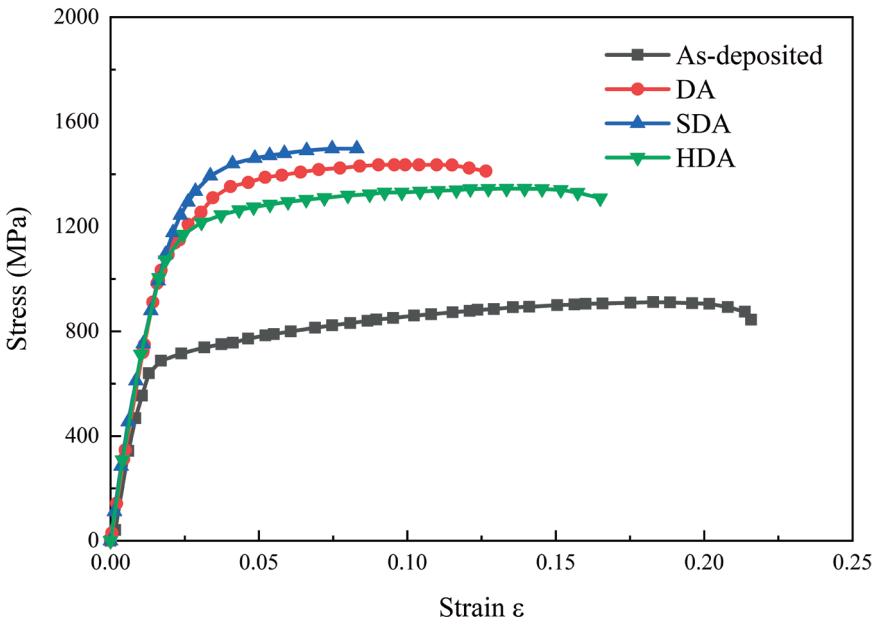


**Figure 11:** Stress–strain curve of the SLM IN718 alloy.

**Table 4:** Mechanical performance of the SLM IN718 alloy.

| SAMPLE | TENSILE STRENGTH (MPa) | FRACTURE ELONGATION (%) | (TENSILE STRENGTH) × (FRACTURE ELONGATION) (GPa%) |
|---|---|---|---|
| As-deposited | 911 | 21.6 | 19.7 |
| DA | 1435 | 12.6 | 18.1 |
| SDA | 1497 | 8.3 | 12.4 |
| HDA | 1345 | 16.5 | 22.2 |

Thus, the volume fraction of the recrystallized and substructure grains can be adjusted by heat treatment to regulate the ductility and strength of the alloy and optimize their mechanical properties.

### 3.3. Fracture morphology

The fracture mode of the SLM IN718 alloy was investigated by observing its fracture morphology using SEM. Figure 12 shows the results of the analysis. The tensile fracture morphology of the SLM IN718 alloy is composed of dimples with different depths and sizes with a ductile fracture mode. Small and shallow dimples are observed in the as-deposited sample, exhibiting a sequential distribution consistent with the large-angle dendritic crystals with epitaxial growth characteristics. This is ascribed to the repeatedly rapid heating and cooling of the IN718 alloy during SLM, resulting in large compositional segregation and residual stresses in the alloy with large defects at the grain boundaries. After heat treatment, the toughness dimples in the three samples became larger and deeper with a more uniform distribution because of the precipitation of the strengthening phases.

### 3.4. Damage evolution

Uniaxial tensile tests were conducted using an MTS-Landmark mechanical property tester and a DIC equipment to investigate the damage deformation of the SLM IN718 alloy. Figure 13 displays the global strain cloud map of the samples at various deformation stages before and after heat treatment. The SLM IN718 alloy enters the plastic stage during the tensile process with heat treatment, and strain-concentration area and uneven deformation appeared in the sample. As the strain-concentration area decreases, a clear necking area is observed on the strain cloud map, and the material damage is concentrated in this area. The apparent damage evolution behavior of the SLM IN718 alloy was quantitatively analyzed using DIC to obtain the strain field data in the experimental loading direction (Y direction). The point-partitioning is shown in Figure 14. A total of 5000 data points, which are ensured to fully cover the entire sample area, was randomly selected from the DIC observation area. Meanwhile, 300 data points, which are ensured to fully cover the deformation-concentration area, were randomly selected in the deformation-concentration area. The average strain $\bar{\varepsilon}$ is defined as:

$$\bar{\varepsilon} = \left| \frac{1}{300} \sum_{i=1}^{300} (\varepsilon_{yy})_i - \frac{1}{5000} \sum_{j=1}^{5000} (\varepsilon_{yy})_j \right| \tag{1}$$

where $\frac{1}{300}\sum_{i=1}^{300}(\varepsilon_{yy})_i$ represents the $\bar{\varepsilon}$ of 300 data points in the strain-concentration area, and $\frac{1}{5000}\sum_{j=1}^{5000}(\varepsilon_{yy})_j$ represents the $\bar{\varepsilon}$ of 5000 data points in the entire strain field.

According to Equation (1), the degree of strain concentration in the SLM IN718 alloy increases as $\bar{\varepsilon}$ increases. Therefore, $\bar{\varepsilon}$ can reflect the apparent damage evolution characteristics of the SLM IN718 alloy. The relationship between $\bar{\varepsilon}$ and macroscopic deformation was quantitatively described from the curve of $\bar{\varepsilon}$ and engineering strain $\varepsilon$ of the SLM IN718 alloy, as shown in Figure 15. Similar variations are noted on the $\bar{\varepsilon}$ and $\varepsilon$ of the SLM IN718 alloy before and after heat treatment, in which $\bar{\varepsilon}$ increases with the increase of $\varepsilon$. During the initial deformation stage, $\bar{\varepsilon}$ as the $\varepsilon$ increases slowly, suggesting the absence of an obvious strain-concentration area. When $\varepsilon$ reaches a certain value, $\bar{\varepsilon}$ rapidly increase, at which a clear strain-concentration area appears.

The degree of damage to the SLM IN718 alloy was further characterized by normalizing $\bar{\varepsilon}$ and defining the damage factor $D$ as follows:

$$D = \bar{\varepsilon} / \bar{\varepsilon}_{max} \tag{2}$$

where $\bar{\varepsilon}_{max}$ is the average strain at fracture. The range of $D$ is between 0 and 1. When $D = 0$, the SLM IN718 alloy is in its initial state without damage. When $0 < D < 1$, the SLM IN718 alloy is in the stretching process,

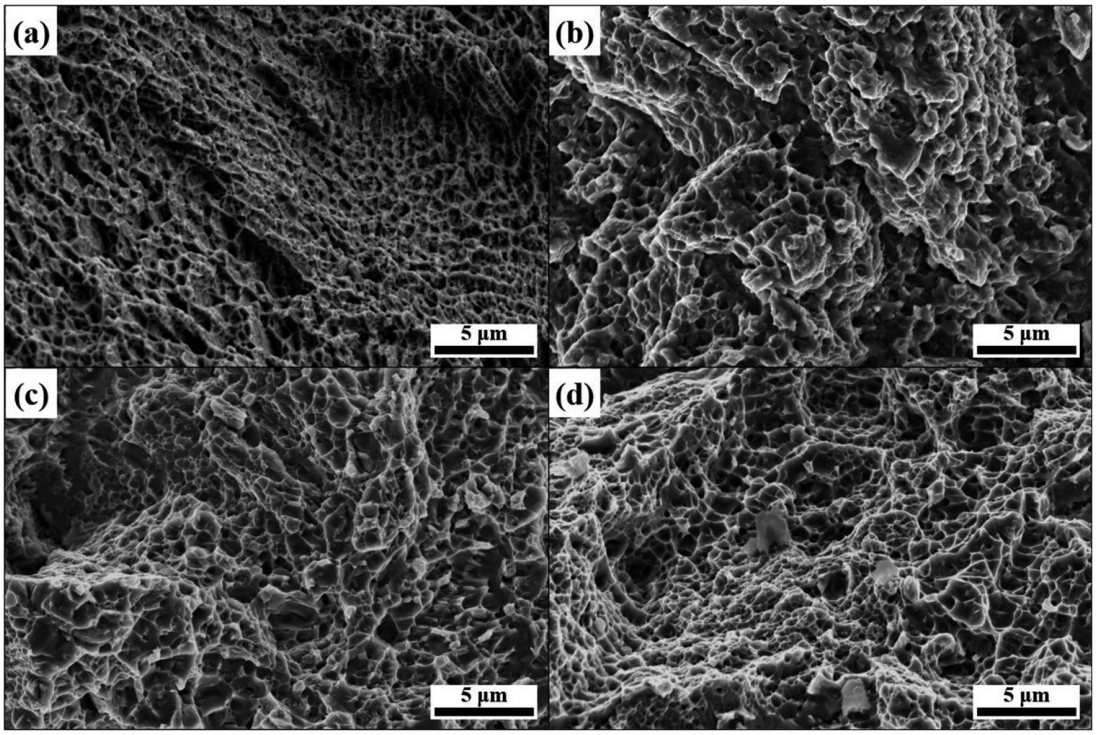


**Figure 12:** Tensile fracture morphology of the SLM IN718 alloy: (a) as-deposited, (b) DA, (c) SDA, and (d) HDA.

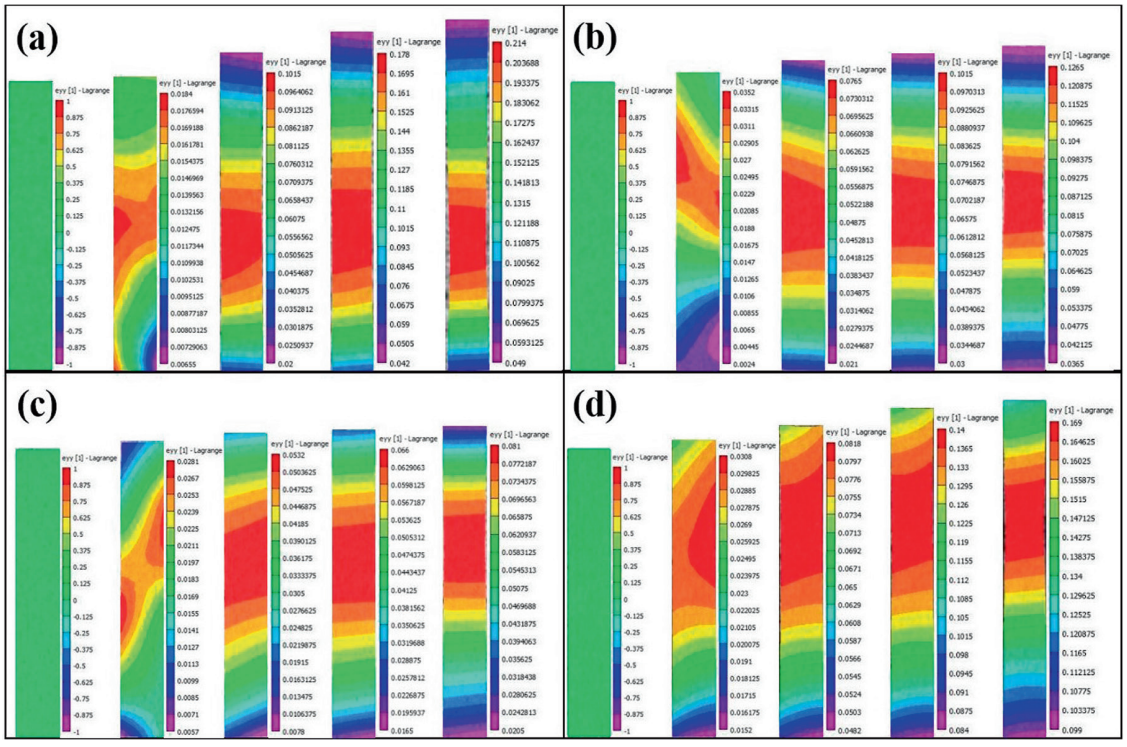


**Figure 13:** Global strain cloud map of the SLM IN718 alloy at various deformation stages: (a) as-deposited, (b) DA, (c) SDA, and (d) HDA.

whereby the degree of damage to the alloy increases with $D$. When $D = 1$, the SLM IN718 alloy fractures and fails. Therefore, the expression transformation of damage from 0 to 1 is obtained by establishing $D$.

The $D$ evolution curve of SLM IN718 alloy is shown in Figure 16. The $D$ of the SLM IN718 alloy before and after heat treatment varies with $\varepsilon$ with the same evolutionary laws. Subsequently, the curvature of the $D$

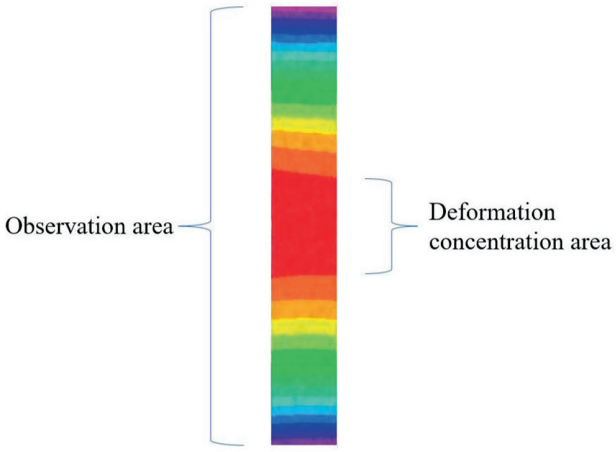


**Figure 14:** Schematic of the point-taking partition.

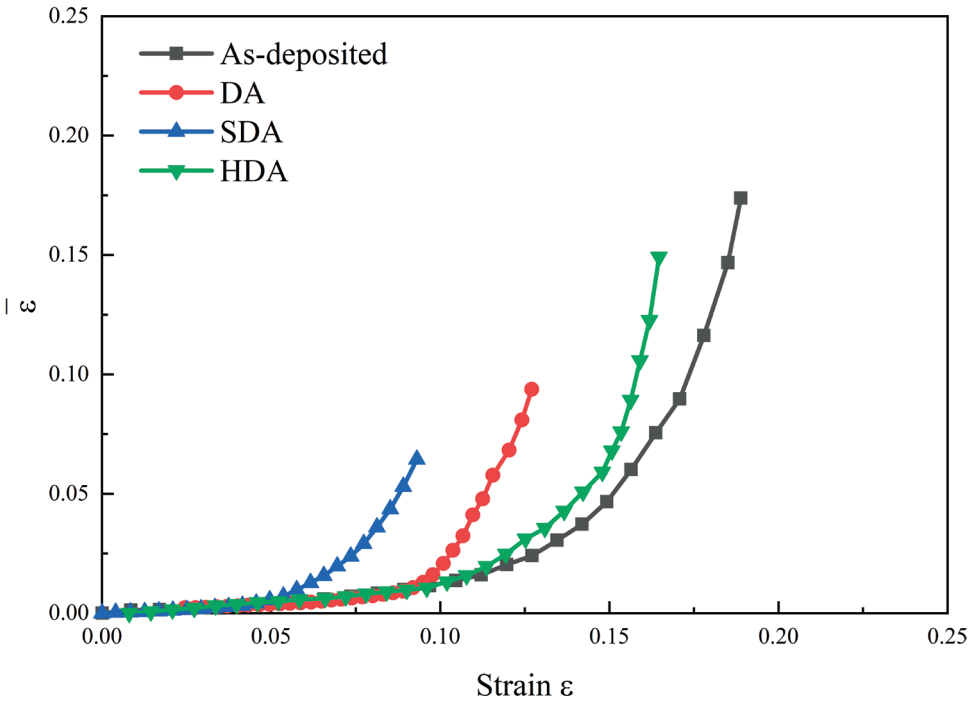


**Figure 15:** Evolution curve of the average strain factor $\bar{\varepsilon}$ of the SLM IN718 alloy.

fitting curve was calculated. The point with the highest curvature is defined as the critical damage factor $D_C$, and the corresponding strain is defined as the critical plastic strain $\varepsilon_C$. The $D_C$ before and after heat treatment is shown in Figure 17. When $0 < D < D_C$, the SLM IN718 alloy is in the early stage of deformation with slow damage accumulation. When $D = D_C$, the damage begins to increase rapidly. The deformation starts to concentrate towards local areas. When $D_C < D < 1$, the damage enters the rapid accumulation stage. When $D = 1$, the SLM IN718 alloy fractures and fails. Figure 17 shows the highest $D_C$ of the as-deposited sample with the latest rapid damage and lowest $D_C$ of the SDA sample with the earliest rapid damage.

By fitting the $D$ of the SLM IN718 alloy with an exponential function, the damage evolution equations of the SLM IN718 alloy are obtained as follow:

As-deposited sample:

$$D = 0.1937\left(\frac{\varepsilon}{0.1564}\right)^{5.3596} \tag{3}$$

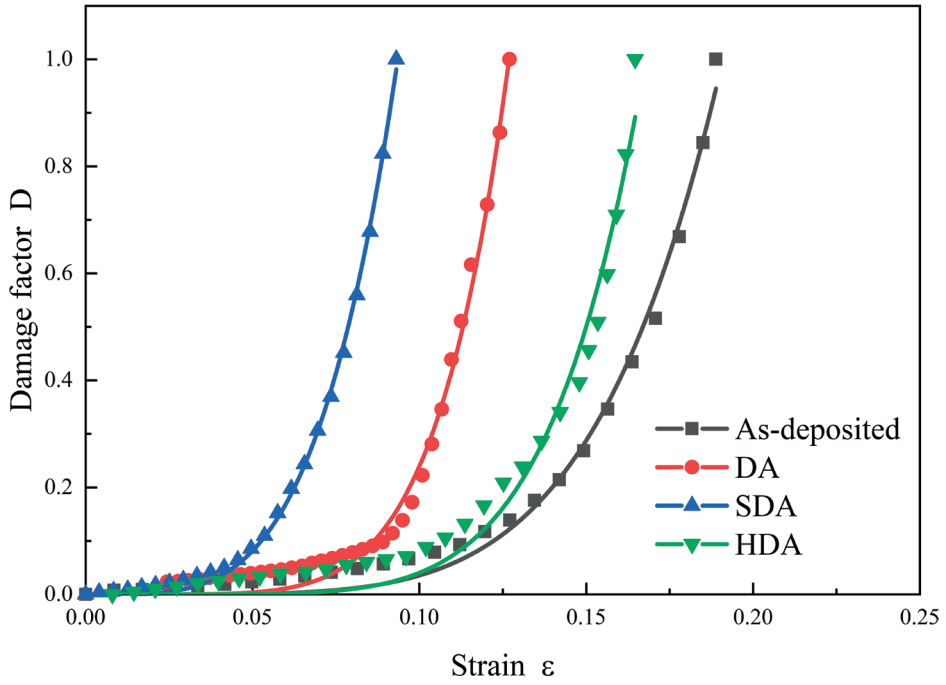


**Figure 16:** Evolution curve of the damage factor *D* of the SLM IN718 alloy.

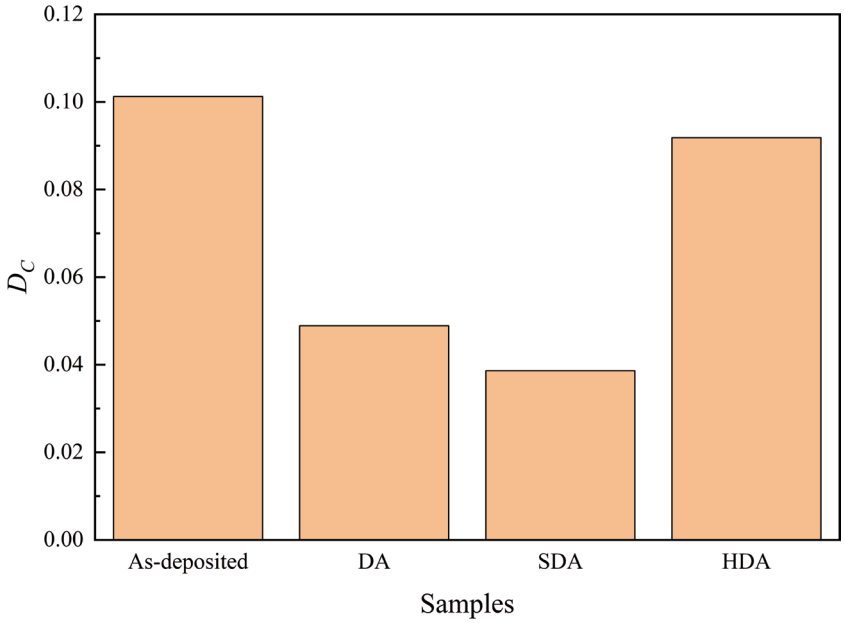


**Figure 17:** Critical damage factor $D_C$ for the SLM IN718 alloy.

DA sample:

$$D = 0.1665\left(\frac{\varepsilon}{0.0937}\right)^{6.2110} \tag{4}$$

SDA sample:

$$D = 0.2497\left(\frac{\varepsilon}{0.0635}\right)^{4.0685} \tag{5}$$

HDA sample:

$$D = 0.1512\left(\frac{\varepsilon}{0.1249}\right)^{6.6161} \tag{6}$$

The fitting equation is then combined to establish the general equation:

$$D = A\left(\frac{\varepsilon}{B}\right)^{C} \tag{7}$$

where $A$ is the plastic damage model parameter, $B$ is the fractured plastic strain, and $C$ is the plastic damage model index.

## 4. CONCLUSIONS

This study investigated the microstructure of the SLM IN718 alloy after different heat treatments. Uniaxial tensile tests were conducted on the SLM IN718 alloy after different heat treatments, and its damage evolution behavior was studied using DIC. The following conclusions were drawn from this work:

(1) After heat treatment, the SLM IN718 alloy underwent varying degrees of recrystallization and the microstructure transformed from dendritic to block crystals. The melt scar gradually disappeared, and large quantities of γ′ and γ″ phases precipitated. With the increase in the heat-treatment temperature, recrystallization was gradually completed. The crystal tended to transform to equiaxial grains with grain coarsening. The δ phase first precipitated and then dissolved. Moreover, the hardness and strength of the SLM IN718 alloy increased and then decreased, the elongation declined and then increased, and toughness fracture was the fracture mode.

(2) The ductility and strength of the alloy can be tuned using the proportion of recrystallized and substructured grains with various heat treatment methods. The recrystallized grains improved the ductility, whereas the substructured grains improved the toughness owing to their high dislocation density. For the HA samples, the proportions of recrystallized and substructured grains were 72.3% and 27.6%, respectively, and the product of strength and elongation was 22.2 GPa%, which can be further optimized in future studies.

(3) The $D$ of the SLM IN718 alloy increased with the increase of $\varepsilon$, and its evolution exhibited slow deformation and rapid damage stages. After heat treatment, $D$ entered the rapid damage stage earlier. As $\varepsilon_C$ increased, $D_C$ increased. The evolutions of $D$ of the as-deposited and HA samples were more similar than those of the other samples. The product of the strength and elongation of the as-deposited and HA samples were 19.7 and 22.2 GPa%, respectively, reflecting the complementary effect of strength and ductility to damage evolution. Finally, a general equation for the damage evolution of the SLM IN718 alloy under different heat treatments was established.

## 5. ACKNOWLEDGMENTS

This work was supported by the National Natural Science Foundation [grant numbers 12262029]; the Doctoral Fund of Inner Mongolia University of Technology [grant numbers BS2021053]; the Inner Mongolia Natural Science Foundation [grant numbers 2023MS01007, 2022MS01009]; and the Inner Mongolia Basic Research Operations [grant numbers JY20230010].

## 6. BIBLIOGRAPHY

[1] ZHANG, C., QIAN, B., ZHANG, L., *et al*., "Research progress of additive manufacturing process, materials and structure", *Machine Tool & Hydraulics*, v. 51, n. 9, pp. 180–196, May. 2023.

[2] AGIUS, D., KOUROUSIS, K., WALLBRINK, C., "A review of the as-built SLM Ti6Al4V mechanical properties towards achieving fatigue resistant designs", *Metals*, v. 8, n. 1, pp. 75, Jan. 2018. doi: http://dx.doi.org/10.3390/met8010075.

[3] KOUTIRI, I., PESSARD, E., PEYRE, P., *et al*., "Influence of SLM process parameters on the surface finish, porosity rate and fatigue behavior of as-built Inconel 625 parts", *Journal of Materials Processing Technology*, v. 255, pp. 536–546, May. 2018. doi: http://dx.doi.org/10.1016/j.jmatprotec.2017.12.043.

[4] TUCHO, M.W., LYSNE, H.V., AUSTBØ, H., *et al*., "Investigation of effects of process parameters on microstructure and hardness of SLM manufactured SS316L", *Journal of Alloys and Compounds*, v. 740, pp. 910–925, Apr. 2018. doi: http://dx.doi.org/10.1016/j.jallcom.2018.01.098.

[5] KHOO, Z.X., LIU, Y., LOW, Z.H., *et al*., "Fabrication of SLM NiTi shape memory alloy via repetitive laser scanning", *Shape Memory and Superelasticity*, v. 4, n. 1, pp. 112–120, Jan. 2018. doi: http://dx.doi.org/10.1007/s40830-017-0139-7.

[6] WANG, Z., GUAN, K., GAO, M., *et al*., "The microstructure and mechanical properties of deposited-IN718 by selective laser melting", *Journal of Alloys and Compounds*, v. 513, pp. 518–523, Feb. 2012. doi: http://dx.doi.org/10.1016/j.jallcom.2011.10.107.

[7] ZHOU, J., HAN, Y., HUANG, S., *et al*., "Effect of different process temperatures on residual stress and nano-hardness of warm laser peened INl718 superalloy", *Chinese Journal of Lasers*, v. 42, n. 7, pp. 85–92, Jul. 2015.

[8] OLIVEIRA, D., SILVA, R.B., ARENCIBIA, R.V., "Evaluation of dimensional deviation in nickel-base, Inconel 718 alloy after grinding under different cooling-lubrication techniques", *Matéria (Rio de Janeiro)*, v. 24, n. 4, pp. e-12481, 2019. doi: http://dx.doi.org/10.1590/s1517-707620190004.0806.

[9] GONZALEZ, Y.E., MENDOZA, J.M., DURÁN, J.R., *et al*., "Effect of printing parameters on mechanical properties and processing time of additively manufactured parts", *Matéria (Rio de Janeiro)*, v. 28, n. 3, pp. e20230111, 2023. doi: http://dx.doi.org/10.1590/1517-7076-rmat-2023-0111.

[10] CAO, Y., BAI, P., LIU, F., *et al*., "Investigation on the precipitates of IN718 alloy fabricated by selective laser melting", *Metals*, v. 9, n. 10, pp. 1128, Oct. 2019. doi: http://dx.doi.org/10.3390/met9101128.

[11] KOHALE, V., JAWADE, S., KAKANDIKAR, G., "Investigation on mechanical behaviour of inconel 718 manufactured through additive manufacturing", *International Journal on Interactive Design and Manufacturing*, v. 17, n. 4, pp. 1645–1651, Feb. 2023. doi: http://dx.doi.org/10.1007/s12008-022-01183-7.

[12] SONG, Z., WANG, D., WU, Z., *et al*., "Ultrahigh cycle fatigue performance of GH4169 alloy by selective laser melting", *Materials for Mechanical Engineering*, v. 44, n. 11, pp. 72–77, Nov. 2020.

[13] HE., S. "Study on microstructure and mechanical properties of IN718 superalloy deposited by laser rapid forming", *Hot Working Technology*, v. 39, n. 21, pp. 197–198, Nov. 2010.

[14] CHLEBUS, E., GRUBER, K., KUŹNICKA, B., *et al*., "Effect of heat treatment on the microstructure and mechanical properties of Inconel 718 processed by selective laser melting", *Materials Science and Engineering A*, v. 639, pp. 647–655, Jul. 2015. doi: http://dx.doi.org/10.1016/j.msea.2015.05.035.

[15] ZHAO, Y., GUO, Q., MA, Z., *et al*., "Comparative study on the microstructure evolution of selective laser melted and wrought IN718 superalloy during subsequent heat treatment process and its effect on mechanical properties", *Materials Science and Engineering A*, v. 791, pp. 139735, Jul. 2020. doi: http://dx.doi.org/10.1016/j.msea.2020.139735.

[16] ZHANG, Q., ZHANG, J., LI, D., *et al*., "Microstructure and properties of laser additive remanufactured IN718 alloy with different aging temperatures", *Rare Metal Materials and Engineering*, v. 49, n. 5, pp. 1785–1792, May. 2020.

[17] PODESTA, L., WATTRISSE, B., LATOURTE, F., *et al*. "In-situ tensile test on 316H SENT using digital image correlation", In: *Proceedings of Springer International Publishing: Experimental and Applied Mechanics*, vol. 4, pp. 45–52, Sept. 2017. doi: http://dx.doi.org/10.1007/978-3-319-42028-8_6.

[18] PISANU, L., BARBOSA, J., BAMBERG, P., *et al*., "Influence of coupling agents on the adhesion force of dissimilar overmolded polymers: a digital image correlation analysis", *Matéria (Rio de Janeiro)*, v. 24, n. 3, pp. e-12438, 2019. doi: http://dx.doi.org/10.1590/s1517-707620190003.0800.

[19] POPOVICH, V.A., BORISOV, E.V., POPOVICH, A.A., *et al*., "Impact of heat treatment on mechanical behaviour of Inconel 718 processed with tailored microstructure by selective laser melting", *Materials & Design*, v. 131, pp. 12–22, Oct. 2017. doi: http://dx.doi.org/10.1016/j.matdes.2017.05.065.

[20] OKEIL, A., MATSUMOTO, K., NAGAI, K., "Investigation on local bond behavior in concrete and cement paste around a deformed bar by using DIC technique", *Cement and Concrete Composites*, v. 109, pp. 103540, May. 2020. doi: http://dx.doi.org/10.1016/j.cemconcomp.2020.103540.

[21] WEI, L., LI, L., CUI, X., *et al*., "Study on damage evolutiong of cu-ni19 alloy at different annealing temperatures based on dic method", *Engineering Mechanics*, v. 37, n. 4, pp. 227–235, Apr. 2020.

[22] SI, G., LI, W., XU, H., *et al*., "Monitor of TC4 alloy fatigue damage based on DIC and acoustic emission technologies", *Journal of Northeast Petroleum University*, v. 44, n. 3, pp. 119–126, Jun. 2020.

[23] GUO, Y., ZHAO, X., BAI, P., *et al*., "Effects of solution treatment on microstructure and hardness of inconel 718 alloy fabricated by selective laser melting", *China Surface Engineering*, v. 34, n. 2, pp. 114–121, Apr. 2021.

[24] CAO, G.H., SUN, T.Y., WANG, C.H., *et al*., "Investigations of γ′, γ″ and δ precipitates in heat-treated Inconel 718 alloy fabricated by selective laser melting", *Materials Characterization*, v. 136, pp. 398–406, Feb. 2018. doi: http://dx.doi.org/10.1016/j.matchar.2018.01.006.

[25] HUANG, L., CAO, Y., ZHANG, J., *et al*., "Effect of heat treatment on the microstructure evolution and mechanical behaviour of a selective laser melted Inconel 718 alloy", *Journal of Alloys and Compounds*, v. 865, n. 16, pp. 158613, Jun. 2021. doi: http://dx.doi.org/10.1016/j.jallcom.2021.158613.

[26] ZHAO, R., ZHAO, Z., BAI, P., *et al*., "Effect of heat treatment on the microstructure and properties of inconel 718 alloy fabricated by selective laser melting", *Journal of Materials Engineering and Performance*, v. 31, n. 1, pp. 353–364, Jul. 2021. doi: http://dx.doi.org/10.1007/s11665-021-06212-2.

[27] SHI, J.J., LI, X., ZHANG, Z.X., *et al*., "Study on the microstructure and creep behavior of Inconel 718 superalloy fabricated by selective laser melting", *Materials Science and Engineering A*, v. 765, pp. 138282, Sep. 2019. doi: http://dx.doi.org/10.1016/j.msea.2019.138282.

[28] ÖZER, S., BILGIN, G.M., DAVUT, K., *et al*., "Effect of post fabrication aging treatment on the microstructure, crystallographic texture and elevated temperature mechanical properties of IN718 alloy fabricated by selective laser melting", *Journal of Materials Processing Technology*, v. 306, pp. 117622, Aug. 2022. doi: http://dx.doi.org/10.1016/j.jmatprotec.2022.117622.

[29] PARK, S., KIM, K., KIM, M., *et al*., "Effect of post-heat treatment on the tensile and cryogenic impact toughness properties of inconel 718 manufactured by selective laser melting", *Advanced Engineering Materials*, v. 23, n. 3, pp. 2001005, Nov. 2021. doi: http://dx.doi.org/10.1002/adem.202001005.